Copper magnetic centers in oxygen deficient $R\mathrm{Ba_2Cu_3O_{6+x}}$ (R=Nd, Sm): An EPR and magnetic study

V. Likodimos and N. Guskos*
Solid State Section, Department of Physics, University of Athens, Panepistimiopolis, GR-15784 Zografos, Athens, Greece

H. Gamari-Seale and A. Koufoudakis
National Center for Scientific Research ''Democritos,'' Aghia Paraskevi Attikis, GR-153 10, Athens, Greece

M. Wabia, J. Typek, and H. Fuks
Institute of Physics, Technical University of Szczecin, A1.Piastow 17, PL-70310 Szczecin, Poland
(Received 5 April 1996)

EPR and magnetic results are reported for oxygen deficient, nonsuperconducting $R\mathrm{Ba_2Cu_3O_{6+x}}$ (R=Nd, Sm) compounds. The magnetic-susceptibility $\chi(T)$ and isothermal $M(H)$ data are analyzed as the superposition of the rare-earth R^{3+} contribution with another strongly ferromagnetic (FM) contribution arising from FM copper clusters with large total spin S. The rare-earth paramagnetic contribution in $\chi(T)$ and $M(H)$ are calculated using the results of consistent crystal-field analysis (intermediate coupling wave functions, J-mixing effects) of Nd^{3+} and Sm^{3+} ions. The corresponding EPR spectra comprise an intense, almost isotropic EPR line whose intensity $I(T)$ exhibits a ferromagnetic behavior, while g_{eff} and the linewidth ΔH_{pp} diverge at $T<10$ K indicating the presence of slowly fluctuating ''internal'' fields. The origin of the FM clusters is related to spin-polarized copper clusters through oxygen holes in the Cu(1) or Cu(2) layers, while the ferromagnetic interaction of the $Cu^{2+}(1)$ with the $Cu^{2+}(2)$ moments may be involved in the low-temperature ($T<10$ K) behavior of the EPR parameters. On increasing the oxygen deficiency, the ferromagnetic contribution is drastically reduced and more isolated Cu^{2+} centers appear as shown by the corresponding EPR data. Exact simulation of the latter anisotropic EPR spectra, shows that the anisotropic linewidths ΔH_i ($i=x,y,z$) gradually broaden at low temperatures, while the intensity $I(T)$ shows antiferromagnetic behavior. EPR measurements on an ''aged'' $\mathrm{Nd_{0.5}Y_{0.5}Ba_2Cu_3O_{6+x}}$ sample revealed that the Cu^{2+} EPR spectrum intensifies with time, a behavior probably related to oxygen ordering processes or to surface degradation effects. Analysis of the EPR resonance of Nd^{3+} and Sm^{3+} ions in combination with the absence of the corresponding EPR spectra indicate the presence of very fast spin-lattice relaxation of the rare-earth ions. [S0163-1829(96)00734-5]

I. INTRODUCTION

There is now considerable experimental evidence leading to the conclusion that copper oxide superconductors and their insulating antiferromagnetic (AFM) parent compounds do not exhibit electron-paramagnetic-resonance (EPR) signals corresponding to the bulk copper ions.[1] Though not conclusive, theoretical studies consider the ''curious'' absence of the Cu^{2+} EPR response as the result of excessive broadening occurring through different relaxation processes either in the metallic or in the antiferromagnetic phase.[1]

On the other hand, magnetic measurements on oxygen deficient $\mathrm{YBa_2Cu_3O_{6+x}}$ compounds ($x<0.4$) have systematically shown the presence of an intrinsic magnetic contribution which was attributed to the oxygen-induced Cu^{2+} moments in the Cu(1) plane.[2–5] Similar behavior has been reported in magnetization studies of oxygen deficient $R\mathrm{Ba_2Cu_3O_{6+x}}$ (R=rare-earth ion) ceramics containing rare earths like Nd, Sm, or Tm.[6–8] In that case, the magnetic response of the $R\mathrm{Ba_2Cu_3O_{6+x}}$ ($R123$) systems at low temperatures ($T<20$ K) was mainly determined by the superposition of the rare-earth contribution with another magnetic component attributed to the presence of a ''diluted'' ferromagnetic phase in the form of isolated clusters. Moreover, EPR investigations on oxygen deficient $R123$ and mixed rare-earth $R_{0.5}R'_{0.5}\mathrm{Ba_2Cu_3O_{6+x}}$ ceramics, have directly shown the presence of intense EPR signals at temperatures below ~50 K with a marked temperature dependence, which complied with the magnetic-susceptibility results.[8–10] Based on the temperature variation of the EPR intensity, it was suggested that these EPR spectra result from pairs of exchange coupled Cu^{2+} ions with relatively low excitation energy of the order of 10 K, while the shift of the resonance line below 10 K was associated with the appearance of magnetic ordering processes.[8]

Low oxygen doping of the insulating AFM $R\mathrm{Ba_2Cu_3O_6}$ phase is expected initially to maintain oxygen holes confined in short copper-oxygen chain fragments in the Cu(1) plane, while further increase of the oxygen concentration results in hole doping of the AFM Cu(2) planes.[11,12] Oxygen holes in the AFM CuO_2 planes are predicted to create immobile ferromagnetic clusters[13] which are the basis for the theoretical model of percolative conducting and superconducting phase formation proposed by Hizhnyakov and Sigmund.[14] Theoretical calculations of the electronic structure of these clusters predict ground states with total spin $S=2$ or $S=3/2$.[15–17] EPR study of fast quenched $\mathrm{La_2CuO_{4+\delta}}$ superconducting samples revealed the presence of strong EPR signals which were attributed to spin-polarized clusters dissociated from

the metallic network.[18] Baranov and Badalyan[19] have also reported the presence of very intense magnetic resonance signals in ceramic and single-crystal $R123$ materials after quenching from high temperatures. These EPR signals were attributed to small magnetic clusters with quasi-one-dimensional structure, while the strong temperature dependence of the g factors was associated with the effect of short-range magnetic order. Recent thulium-''enhanced'' NMR experiments in $TmBa_2Cu_3O_{6+x}$ have shown that the ^{169}Tm nuclear spin-lattice relaxation at temperatures $T<4.2$ K is determined by paramagnetic centers in the CuO_2 double layers, which behave as an AFM singlet-triplet system with an energy gap of the order of 1 K.[20,21] In this respect, it becomes evident that EPR investigations which directly probe any paramagnetic centers, can be very useful in the detection and study of copper magnetic centers in the $R123$ systems.

In this work, we present results of a magnetic and a detailed EPR study of oxygen deficient $RBa_2Cu_3O_{6+x}$ (R=Nd, Sm) ceramics, which provide evidence for the presence of copper magnetic centers and elucidates their magnetic behavior in combination with the degree of deoxygenation. Calculation of the paramagnetic contribution of the rare-earth sublattice is performed using crystal-field analysis of the energy spectrum of Nd^{3+} and Sm^{3+} ions, in order to trace any possible contribution of copper paramagnetic centers in the bulk magnetization of the $R123$ systems, while a brief analysis of the Nd^{3+} and Sm^{3+} EPR resonance is also given indicating the presence of very rapid spin relaxation for these ions.

II. EXPERIMENTAL DETAILS

Oxygen defient polycrystalline ceramic samples $RBa_2Cu_3O_{6+x}$ (R=Nd, Sm) and one $Nd_{0.5}Y_{0.5}Ba_2Cu_3O_{6+x}$ sample were prepared by annealing the corresponding high-quality superconducting ceramics ($x\approx0.95$, $T_c\approx93$ K), at 850 °C in He atmosphere followed by fast quenching at room temperature in the reducing atmosphere. Higher degree of deoxygenation was obtained by changing the time of high-temperature annealing from 4 h (samples A) to 24 h (samples B). According to thermogravimetric analysis for the less oxygen deficient sample A, the value of x is estimated to be approximately 0.3, which reduces to $\sim$0.15 for the more oxygen deficient samples B. The samples were characterized with powder x-ray diffraction (XRD) using a D500 Siemens diffractometer employing Cu $K\alpha$ radiation. XRD characterization showed that in all cases the samples had tetragonal crystal structure. Only traces of the impurity phase $BaCuO_{2+x}$ were detected for the $RBa_2Cu_3O_{6+x}$ samples, while no indication of impurity phase was detected for the $Nd_{0.5}Y_{0.5}Ba_2Cu_3O_{6+x}$ sample. Magnetic measurements were performed on densely packed powder samples using a PAR 155 vibrating sample magnetometer in the temperature range 4.2–200 K and magnetic-field range 0–2 T. All the investigated samples were found to be nonsuperconducting down to 4.2 K. EPR measurements were carried out using an X-band Bruker 200D spectrometer with 100 KHz modulation. The magnetic field was scaled with an NMR magnetometer, while an Oxford flow cryostat was employed for measurements in the temperature range 3.6–70 K. Measurements were performed in fine powder samples sealed in quartz tubes under the flow of helium gas.

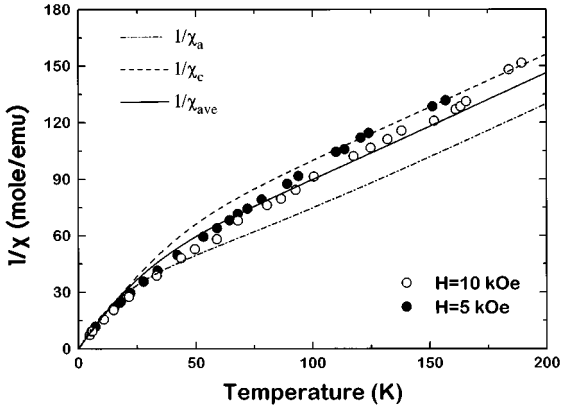

FIG. 1. The inverse magnetic susceptibility $1/\chi$ as a function of temperature for the $NdBa_2Cu_3O_{6+x}$ sample (A) at magnetic fields of 5 and 10 kOe. The lines correspond to the calculated $1/\chi$ curves for Nd^{3+} ions according to the CF analysis.

III. RESULTS AND ANALYSIS

A. Magnetic susceptibility and magnetization

The inverse magnetic susceptibility $1/\chi$ of the $NdBa_2Cu_3O_{6+x}$ sample (A) in magnetic fields of 5 and 10 kOe is shown in Fig. 1, where a slight field dependence of $\chi(T)$ can be traced. In order to investigate the origin of the observed susceptibility we have studied the contribution of the Nd^{3+} sublattice. Neutron diffraction and specific heat measurements have shown that Nd^{3+} ions order antiferromagnetically at low temperatures with a marked dependence of T_N ($\approx$0.5–1.5 K) on the oxygen concentration.[22] However, the magnetic interactions of Nd^{3+} ions have been found to be rather weak ($J/k_B\leqslant2.3$ K, see Ref. 23) to have a significant effect on the magnetic susceptibility in the investigated temperature range (4.2–200 K), and thus in the following we consider Nd^{3+} ions in the paramagnetic regime. In this case, the magnetic response of Nd^{3+} is determined by the Nd^{3+} energy states resulting from the crystal-field (CF) interaction.

The rare-earth point group in the $R123$ tetragonal crystal structure ($P4/mmm$) is D_{4h} so that the crystal-field Hamiltonian acting on the energy terms of the free R^{3+} ions takes the form

$$H_{\mathrm{CF}}=\sum_i B_2^0C_2^0+B_4^0C_4^0+B_4^4(C_4^4+C_4^{-4})+B_6^0C_6^0 + B_6^4(C_6^4+C_6^{-4}), \quad (1)$$

where C_k^q are one-electron irreducible tensor operators, B_k^q are the CF parameters, and the sum runs over the $i4f$ electrons of the R^{3+} ion. The matrix elements of H_{CF} can be calculated using standard tensor operator techniques, while it is important to use intermediate coupling wave functions of the free R^{3+} ions, which are linear combination of Russell-Saunders energy terms characterized by constant total angular momentum J.[24]

The CF parameters for Nd^{3+} ions as a function of the oxygen concentration x in the $NdBa_2Cu_3O_{6+x}$ matrix have

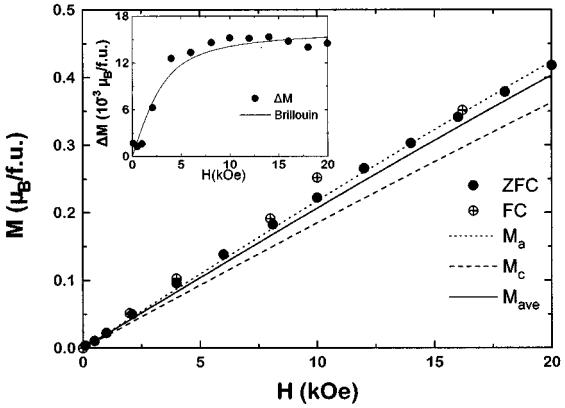

FIG. 2. Magnetization vs applied magnetic field for Nd123 sample (A) at $T=4.8$ K in the ZFC and FC modes. The lines correspond to the calculated $M(H)$ curves for Nd^{3+} ions in tetragonal CF symmetry along the a and c crystallographic axes and the average value $M_{\rm ave}$. The inset shows the $\Delta M(H)$ data derived by $\Delta M=M_{\rm exp}-M_{\rm ave}$. The solid line corresponds to fitting of $\Delta M(H)$ data using the Brillouin function $M_s(H/T)=M_0B_s(gS\mu_BH/k_BT)$ with $g=2.0$, $T=4.8$ K and the fitted values $M_0=0.016(3)\mu_B$/f.u. and $S=24(4)$.

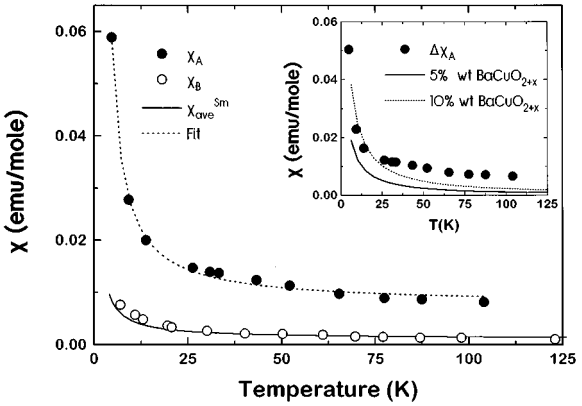

FIG. 3. The magnetic susceptibility $\chi(T)$ for the oxygen deficient Sm123 samples A (solid circles) and B (open circles). The solid line corresponds to the calculated average $\chi_{\rm ave}(T)$ susceptibility for Sm^{3+} ions in tetragonal CF symmetry. The dotted line corresponds to the Curie-Weiss relation $\chi(T)=\chi_0+C/(T-\Theta)$ fitting of $\chi_A(T)$ with $\chi_0=7.7(4)\times10^{-3}$ emu/mole, $\Theta=1.6(2)$ K and $C=0.16(1)$ emu K/mole. The inset shows the difference $\Delta\chi_A=\chi_A-\chi_{\rm ave}$ (solid circles) in comparison with the magnetic susceptibility of 5 (solid line) and 10 (dotted line) wt. % of deoxygenated $BaCuO_{2+x}$ converted in emu/mole Sm123.

been determined by neutron spectroscopy.[25] In the present case, we have used the CF parameters reported for the tetragonal crystal structure of Nd123.[25] Due to the relatively large CF splitting, we have included in the calculation nondiagonal elements (J mixing) of $H_{\rm CF}$ (1) among the three lowest free-ion states ($J=9/2$, 11/2, 13/2) of Nd^{3+} in the intermediate coupling scheme.[26] Diagonalizing $H_{\rm CF}$ (1) we have derived the energy eigenvalues and eigenfunctions which in turn were used to calculate the magnetic susceptibility parallel (χ_c) and perpendicular (χ_a) to the crystallographic c axis, according to the Van Vleck formula[27]

$$\chi_\alpha=\frac{N\mu_B^2}{Z}\sum_{n,i}\left[\frac{\Sigma_j|\langle\phi_{n,i}|L_\alpha+2S_\alpha|\phi_{n,j}\rangle|^2}{k_BT}-2\sum_{j,m\neq n}\frac{|\langle\phi_{n,i}|L_\alpha+2S_\alpha|\phi_{m,j}\rangle|^2}{E_n-E_m}\right]\exp\left[\frac{-E_n}{k_BT}\right], \quad (2)$$

where $\alpha=x$, y, z, and $Z=\Sigma_n d_n\exp(-E_n/k_BT)$ is the partition function with $\Phi_{n,i}$ being the d_n degenerate eigenfunctions with energy E_n at zero magnetic field. Since the magnetic-susceptibility measurements have been carried out on powder samples, the average value $\chi_{\rm ave}=(2\chi_{ab}+\chi_c)/3$ is subsequently used.

The calculated susceptibilities after correcting for the diamagnetic contribution $\chi_{\rm dia}=-2\times10^{-4}$ emu/mole and a temperature-independent contribution from the Cu(2) planes ($\chi_{\rm Cu(2)}=-4\times10^{-4}$ emu/mol),[28] are shown in Fig. 1. The theoretical powder susceptibility $\chi_{\rm ave}$ compares well with the experimental data, indicating that the Nd^{3+} paramagnetic contribution determines to a great extend the bulk magnetic response of Nd123. In order to investigate any field dependence of $\chi(T)$, we have measured the isothermal magnetization curve $M(H)$ with $H\leqslant20$ kOe at $T=4.8$ K in the zero-field-cooled (ZFC) and the field-cooled (FC) mode. The results are presented in Fig. 2, showing that $M(H)$ exhibits a very slight curvature with increasing magnetic field and no appreciable hysteresis. In order to clarify this behavior, the theoretical isotherms $M(H)$ of the Nd^{3+} sublattice were calculated conventionally from diagonalization of a Hamiltonian comprising $H_{\rm CF}$ (1) and the Zeeman interaction, $H_Z=\mu_B(L+2S)H$. The theoretical isotherms M_a, M_c, and the average $M_{\rm ave}=(2M_a+M_c)/3$, at $T=4.8$ K, are shown in Fig. 2. Comparison of the average $M_{\rm ave}$ curve with $M_{\rm exp}$, shows that $M_{\rm ave}$ is somewhat lower than $M_{\rm exp}$. The difference $\Delta M=M_{\rm exp}-M_{\rm ave}$ as shown in the inset of Fig. 2, exhibits a steep increase at low fields saturating already at $H>8$ kOe. This behavior is characteristic of clusters possessing ferromagnetic ground states with large total spin $S>1/2$ and can not be reproduced merely by changing the CF parameters of Nd^{3+} ions. Fitting of the $\Delta M(H)$ data can be performed using the Brillouin function $M_s(H/T)=M_0B_s(gS\mu_BH/k_BT)$ which applies in the case of ferromagnetic clusters with saturation magnetization $M_0=N_{\rm eff}gS\mu_B$, where $N_{\rm eff}$ is the number of clusters per formula unit (f.u.) with total spin S. Fitting of $\Delta M(H)$ with $g=2.0$ and $T=4.8$ K, yields $M_0=0.016(3)\mu_B$/f.u., $S=24(4)$, and $N_{\rm eff}=0.000\,35(6)$ clusters/f.u. (inset of Fig. 2). These results suggest the presence of particularly large ferromagnetic clusters of low concentration at $T=4.8$ K. However, the limited experimental accuracy of the magnetization data inhibits the reliability of the $\Delta M(H)$ curve and thus the absolute values of the fitting parameters (e.g., the surprisingly high value of S) should be considered with caution. Moreover, as we shall see below the obtained fitting values may comprise an appreciable contribution from traces of $BaCuO_{2+x}$. It is also worth noting that a significant ferromagnetic contribution at low temperatures ($T=0.1-7$ K) has been previously reported at low magnetic fields in oxygen deficient $NdBa_2Cu_3O_{6+x}$ ceramics.[7]

The magnetic susceptibility for the oxygen deficient $SmBa_2Cu_3O_{6+x}$ samples A and B at magnetic fields of 1 and 5 kOe are shown in Fig. 3. As can be seen, the magnetic susceptibility $\chi_A(T)$ for the less oxygen deficient sample A

TABLE I. Crystal-field parameters for Sm^{3+} ions in $SmBa_2Cu_3O_{6+x}$ (in cm^{-1}). In the second row the values of B_k^q predicted by the superposition model are also included.

B_2^0	B_4^0	B_4^4	B_6^0	B_6^4	Ref.
408	−2338	1338	580	1705	This work
	−2737	1543	829	1732	31

exceeds considerably $\chi_B(T)$ for the strongly deoxygenated sample B. Fitting of the magnetic susceptibility $\chi_A(T)$ with a Curie-Weiss law, $\chi(T)=\chi_0+C/(T-\Theta)$, gives $\chi_0=7.7(4)\times10-3$ emu/mole, $\Theta=1.6(2)$ K, and $\mu_{\rm eff}=1.12(5)\mu_B/Sm^{3+}$, the latter being significantly higher than the $\mu_{\rm eff}$ value ($0.84\mu_B$) of the free ion Sm^{3+}. To clarify this discrepancy we performed CF analysis for Sm^{3+} ions in the Sm123 matrix and subsequently calculated the magnetic susceptibility as in the case of Nd^{3+} ions. Due to the large neutron absorption cross section of Sm^{3+}, inelastic neutron scattering cannot be used for the determination of the CF energy levels in Sm123.[29] In order to obtain an estimate of the Sm^{3+} CF energy states, we have consistently scaled the CF parameters B_k^q that have been reported for other R^{3+} ions in the $R123$ matrix using the scaling procedure developed by Morrison and Leavitt[30] and keeping the ratios of B_k^q as predicted by the superposition model.[31] The resulting CF parameters B_k^q for the tetragonal symmetry are listed in Table I.

Due to the relatively small energy separation of the lowest ^6H_J free-ion states of Sm^{3+} as is often the case for the lighter lanthanides, we have included in the CF analysis the first five J multiplets ($J=5/2-13/2$) of Sm^{3+} in the intermediate coupling scheme[32] allowing for J mixing. A similar consistent approach of Sm^{3+} has been already reported by Soderholm *et al.*,[29] though the CF parameters and the resulting energy states were not reported. The eigenvalues and eigenstates of the ground multiplet of Sm^{3+} ions in tetragonal symmetry, $H_{\rm CF}$ (1), derived in the present work are listed in Table II.

Using relation (2), the magnetic susceptibilities χ_a, χ_c, and $\chi_{\rm ave}$ of Sm^{3+} in the paramagnetic regime were calculated. The derived average susceptibility $\chi_{\rm ave}$ after correction for diamagnetic and Cu(2) contribution, is compared with the experimental data in Fig. 3, where we find that good agreement is obtained for sample B in most of the investigated temperature range, except for temperatures $T<25$ K where $\chi_{\rm exp}$ slightly exceeds the theoretical curve. This result indicates that the CF parameters used in this work are a good approximation for the Sm^{3+} crystal-field interaction. However, the magnetic susceptibility for sample A is significantly larger than the predicted $\chi_{\rm ave}$. The observed difference $\Delta\chi=\chi_A-\chi_{\rm ave}$ is shown in the inset of Fig. 3. Since the Sm123 samples, according to the XRD analysis, contained traces ($\leqslant3\%$) of the barium cuprate oxide $BaCuO_{2+x}$, we compare the difference $\Delta\chi$ with the magnetic susceptibility of oxygen deficient $BaCuO_{2+x}$. Magnetic-susceptibility data for deoxygenated $BaCuO_{2+x}$ have been recently reported by Gouskos *et al.*[33] As shown in the inset of Fig. 3, the presence of $BaCuO_{2+x}$ assuming concentration as large as 10 wt. % cannot fully account for the observed $\Delta\chi$.

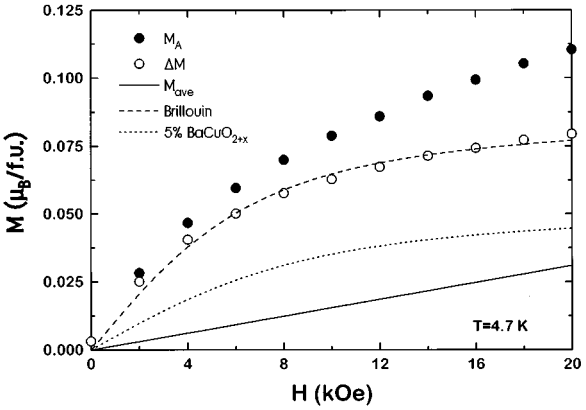

FIG. 4. Magnetization vs applied magnetic field for Sm123 sample (A) at $T=4.7$ K (solid circles) in comparison with the $M_{\rm ave}(H)$ (solid line) calculated for Sm^{3+} ions according to the CF analysis. Open circles show the difference $\Delta M=M_A-M_{\rm ave}$ which is fitted with the Brillouin function (dotted line) with $M_0=0.086(5)\mu_B$/f.u., $S=12(1)$. The dashed line represents the isotherm $M(H)$ calculated for $BaCuO_{2+x}$ at $T=4.7$, according to the results of Ref. 34.

Figure 4 shows the isotherm $M_A(H)$ for the Sm123 sample A at $T=4.7$ K. In the same plot, the calculated $M_{\rm ave}(H)$ of the Sm^{3+} ions is shown. Similar to the magnetic-susceptibility behavior, $M_A(H)$ exceeds significantly the Sm contribution $M_{\rm ave}$ and exhibits a pronounced curvature indicative of ferromagnetic behavior. The difference $\Delta M=M_A-M_{\rm ave}$ is fitted with the Brillouin function appro-

TABLE II. CF eigenvalues (E) and eigenstates of the ground multiplet of Sm^{3+} ions in D_{4h} symmetry of $SmBa_2Cu_3O_{6+x}$.

E (cm^{-1})	Γ_i	Eigenfunctions
0	Γ_6	$0.986\|5/2,\pm1/2\rangle\pm0.069\|7/2,\pm1/2\rangle\pm0.039\|7/2,\mp7/2\rangle$ $-0.036\|9/2,\pm1/2\rangle-0.123\|9/2,\mp7/2\rangle+0.0125\|9/2,\pm9/2\rangle$ $\pm0.006\|11/2,\pm1/2\rangle\pm0.021\|11/2,\mp7/2\rangle\mp0.061\|11/2,\pm9/2\rangle+\cdots$
171	$\Gamma_7^{(1)}$	$0.640\|5/2,\pm5/2\rangle-0.727\|5/2,\mp3/2\rangle\pm0.144\|7/2,\pm5/2\rangle\pm0.156\|7/2,\mp3/2\rangle$ $+0.087\|9/2,\pm5/2\rangle+0.069\|9/2,\mp3/2\rangle$ $\mp0.046\|11/2,\pm5/2\rangle\mp0.037\|11/2,\mp3/2\rangle\pm0.018\|11/2,\mp11/2\rangle+\cdots$
371	$\Gamma_7^{(2)}$	$0.745\|5/2,\pm5/2\rangle+0.571\|5/2,\mp3/2\rangle\mp0.278\|7/2,\pm5/2\rangle\mp185\|7/2,\mp3/2\rangle$ $+0.036\|9/2,\pm5/2\rangle+0.055\|9/2,\mp3/2\rangle$ $\mp0.004\|11/2,\pm5/2\rangle\mp0.037\|11/2,\mp3/2\rangle\mp0.011\|11/2,\mp11/2\rangle+\cdots$

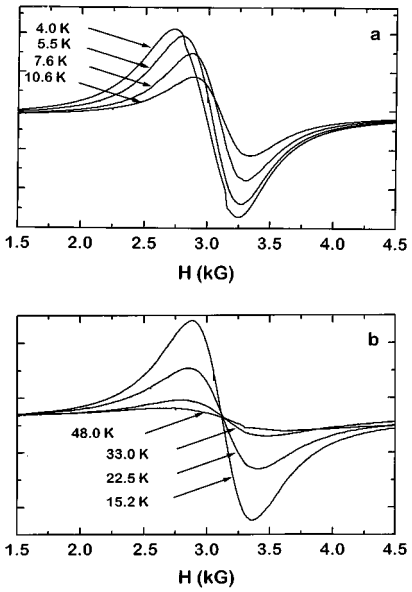

FIG. 5. Temperature dependence of the X-band (ν=9.43 GHz) EPR spectrum of Nd123 sample (A) at (a) $T<10$ K and (b) $T>10$ K.

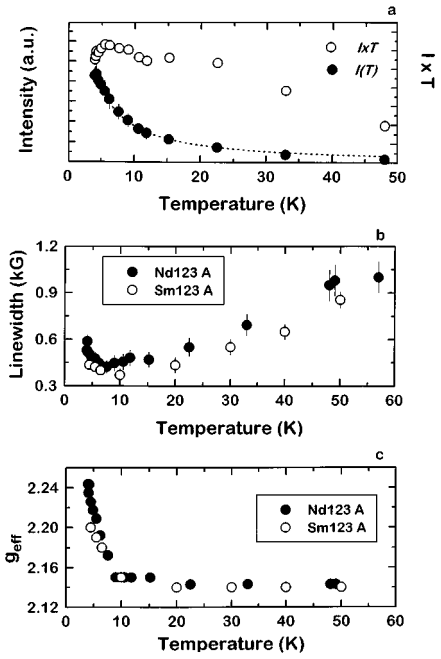

FIG. 6. Temperature dependence of the isotropic EPR line parameters, (a) $I(T)$, $I\times T$ and the fitting function $I(T)\approx 1/T[3+\exp(-J/k_BT)]$ (dotted line) with ferromagnetic exchange constant $J/k_B\approx 30(15)$ K, (b) peak-to-peak linewidth, and (c) g_{eff} for the Sm123 and Nd123 samples (A). In the intensity plot only data for Nd123 are shown.

priate for the ground-state magnetization of a ferromagnetic cluster as in the case of Nd123 sample A, yielding $M_0=0.086(5)\mu_B$/f.u., $S=12(1)$ and $N_{\text{eff}}=0.0036(2)$ clusters/f.u. In Fig. 4 it is also included the isotherm $M(H)$ calculated for $BaCuO_{2+x}$ at $T=4.7$, according to the magnetization results of Wang *et al.*,[34] who have shown that the low-temperature magnetization of the barium cuprate oxide is mainly determined by the contribution of the large ferromagnetic $Cu_{18}O_{24}$ clusters with total spin $S=9$. As seen in Fig. 4, assuming 5 wt. % of barium cuprate, only part of ΔM is accounted for. In this case, the magnitude of $\Delta M(H)$ can be accounted for by a concentration of $\sim$10 wt. % of the $BaCuO_{2+x}$ magnetization, which however is not in agreement with the XRD results. In the case of Nd123 sample A the smaller magnitude of $\Delta M(H)$ can be accounted for, already by 2 wt. % of $BaCuO_{2+x}$. However, the previous magnetic-susceptibility data and the EPR results presented below, do not comply merely with the presence of barium cuprate. Morever, the XRD analysis did not show any significant change of the $BaCuO_{2+x}$ traces among the two kind of Sm123 samples where the ferromagnetic contribution in $\chi(T)$ increased drastically. In this respect, we conclude that the observed low-temperature magnetic behavior has an intrinsic ferromagnetic origin, though a partial contribution of $BaCuO_{2+x}$ cannot be excluded.

Previous low-temperature magnetization study of oxygen deficient $SmBa_2Cu_3O_{6+x}$ ($x=0.3-0.55$) ceramics showed a maximum of the susceptibility below 1 K, which was associated with the appearance of a small amount of ferromagnetic phase distributed in the sample in the form of clusters.[8] The magnetization $M(H)$ reported at 0.2 K for $SmBa_2Cu_3O_{6+x}$ $x=0.3$, exhibited a steep rise at weak fields saturating for $H=1$ kOe, a behavior which was attributed to the spontaneous magnetization of ferromagnetic clusters and further is in agreement with the present results.

B. EPR results

Figure 5 shows the temperature dependence of the X-band EPR spectrum of the Nd123 sample A below 50 K. The spectrum is dominated by a very intense almost isotropic EPR line of Lorentzian line shape indicative of exchange narrowing. Characteristic of the strong intensity of this EPR line is that it has been recorded under the lowest spectrometer gain and low microwave power of 1 mW, which are almost the same conditions as those used in recordering the intense EPR spectra of powder $BaCuO_{2+x}$ samples.[33] The EPR line narrows rapidly with decreasing temperature and below $T\sim 10$ K shifts towards lower fields. The same kind of EPR spectrum with similar temperature variation and intensity was detected for the Sm123 sample A, as well. The temperature variation of the intensity I which was derived by double integration of the first derivative mode after correcting for baseline shift, the peak-to-peak linewidth ΔH_{pp} and the g_{eff} factor are shown in Fig. 6 for the Nd123 and Sm123 samples A, respectively.

Analysis of the integral intensity $I(T)$ for the Nd123 sample A [Fig. 6(a)] which is proportional to the spin susceptibility, shows that $I(T)$ increases more rapidly with decreasing temperature than T^{-1} which is expected for a simple paramagnetic center with spin $S=1/2$ as Cu^{2+} ions. This behavior, which implies ferromagnetic interactions, can be more easily traced in the plot $I\times T$ shown in Fig. 6(a), where $I\times T$ exhibits a considerable increase down to 6 K, where it reaches a maximum. The intensity $I(T)$ at $T>5$ K can be approximately described with relation $I(T)\approx 1/T[3+\exp(-J/k_BT)]$ which applies for a singlet-triplet system resulting from the exchange interaction of two $S=1/2$ species as two Cu^{2+} ions, with J being the isotropic exchange constant. The derived value of the exchange constant after fitting the experimental data, is $J/k_B\approx 30(15)$ K

which is indicative of appreciable ferromagnetic interactions. However, the maximum at $T\sim 6$ K and the subsequent decrease of $I\times T$ at lower temperatures, indicate the presence of weaker antiferromagnetic interactions as well. Thus, it is possible that the spin system giving rise to the EPR line is not simply a copper dimer but a larger copper cluster with competing ferromagnetic and antiferromagnetic interactions with the former being dominant. In this case, the fine structure expected for ground states with total spin $S>1/2$ induced by anisotropic interactions like the dipolar or the anisotropic/antisymmetric exchange interaction should be exchange narrowed and thus contribute only to the second moment of the resonance line which is thus broadened.

The linewidth $\Delta H_{\rm pp}$ increases almost linearly with temperature above $T\sim 10$ K as seen in Fig. 6(b), with a slope $d(\Delta H_{\rm pp})/dT$ of 12(1) G/K, 13(1) G/K and residual widths of 220(30) G, 285(35) G for Sm123 and Nd123, respectively. This behavior may be associated with very rapid spin-lattice-relaxation processes which are expected to occur in exchange coupled systems where the resulting spin states may provide more effective relaxation pathways.[35] Moreover, in the case of clusters larger than dimers, fast relaxation may occur through modulation of the isotropic exchange interaction which given a considerable magnitude may be very effective. Linear temperature dependence of $\Delta H_{\rm pp}$ has been often detected in lower dimensional systems and is usually connected with the phonon modulation of the antisymmetric or anisotropic exchange interactions.[36] However, for transition metals like Cu^{2+} where the orbital contribution to the ground state is severely quenched, the latter interactions are rather small and give rise to $d(\Delta H_{\rm pp})/dT$ usually smaller than 1 G/K.[36]

Furthermore, $\Delta H_{\rm pp}$ shows a definite minimum at $T\sim 8$ K and increases rapidly at lower temperatures [Fig. 6(b)], while in the same temperature range, $g_{\rm eff}$ exhibits a considerable increase [Fig. 6(c)]. This behavior can be phenomenologically explained in terms of a fluctuating internal field which add to the applied field altering the resonance condition, while at the same time slowing down of the fluctuation rate of this field may produce a progressive broadening of the resonance line as the temperature decreases. The occurrence of such fluctuating fields might be traced either to short-range order among the spin clusters or to the presence of magnetic interactions of the spin clusters with other spin systems. The temperature dependence of the EPR frequency has been treated theoretically for one-dimensional Heisenberg magnets where it was shown that the g shift originates from the anisotropy of the magnetic susceptibility induced by the dipolar interaction or single-ion anisotropy.[37] Considering the presence of spin clusters with $S>1/2$, then shift of the resonance frequency induced by the exchange interaction may be considerably enhanced by the zero-field splitting of the ground state.

According to these results we suggest that the single resonance line observed in the oxygen deficient Nd123 and Sm123 samples results from ferromagnetic clusters formed by the exchange coupling of two or more Cu^{2+} ions and which at low temperature may be short-range ordered. Similar EPR spectra have been previously reported in oxygen deficient $R123$ ceramics,[9,10] while magnetic resonance data

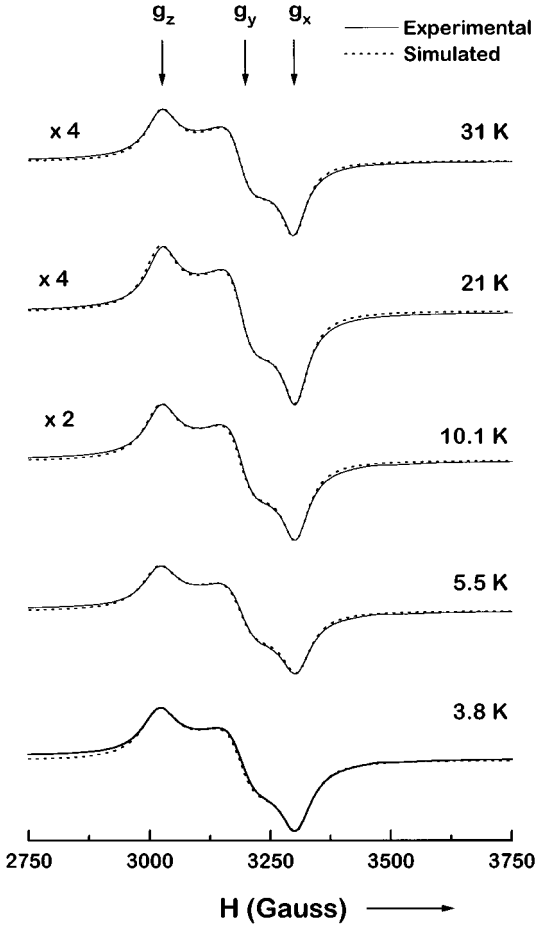

FIG. 7. The anisotropic Cu^{2+} EPR spectra of Sm123 sample (B) as a function of temperature (solid lines). Dotted lines show the theoretical EPR spectra obtained from the simulation with MONOQF.

on oxygen deficient $R123$ single crystals[19] have shown the presence of intense signals with small anisotropy parallel ($g_{\parallel}\sim 2.13$) and perpendicular to the c axis ($g_{\perp}\sim 2.18$) with $g_{\rm eff}\sim 2.16$ at X band and $T>10$ K, which compares favorably with the present $g_{\rm eff}$ values and the small deviation of the observed line shape from an isotropic Lorentzian. EPR spectra with qualitatively similar temperature variation of $g_{\rm eff}$ and $\Delta H_{\rm pp}$ have been also reported for $BaCuO_{2+x}$.[33,38] However, comparison of the intensity of the present EPR signals with that of $BaCuO_{2+x}$ shows that they are of comparable magnitude, while the absolute values of the EPR parameters and their temperature variation are different, excluding any correlation of the origin of the observed EPR spectra with $BaCuO_{2+x}$.

Figure 7 shows the temperature dependence of the EPR spectrum recordered for sample Sm123 B. In this case, a radical change of the EPR spectrum occurred as the isotropic EPR line was replaced by an anisotropic powder EPR spectrum. The integral intensity of this EPR spectrum was greatly reduced, at least by an order of magnitude, in comparison with the intensity of the isotropic EPR line observed in sample Sm123 A, complying with the corresponding reduction of the bulk magnetic susceptibility. The EPR powder pattern is characteristic of Cu^{2+} ions with anisotropic g tensor, while the hyperfine structure expected from the natural isotope ^{63}Cu ($I=3/2$) is suppressed, presumably due to the

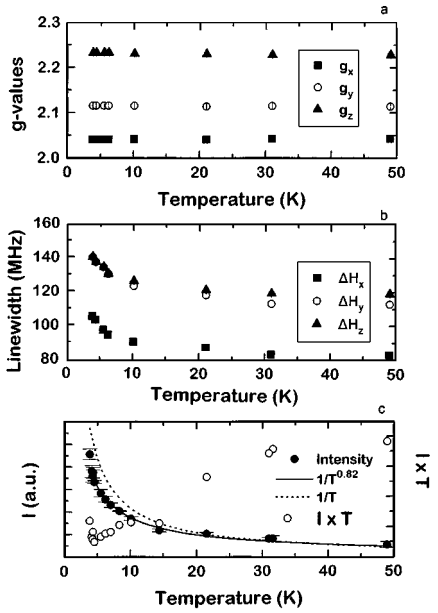

FIG. 8. Temperature dependence of the EPR parameters derived from the simulation of the anisotropic Cu^{2+} EPR spectrum for Sm123 sample (B), (a) the principal g_i values ($i=x, y, z$), (b) the linewidths ΔH_i ($i=x, y, z$) along the principal axes, and (c) the intensity $I(T)$ (solid circles) and $I\times T$ (open circles). The solid and dotted lines correspond to the functions $T^{-0.82}$ and T^{-1}.

presence of weak exchange interactions. The EPR spectrum was theoretically simulated as a function of temperature with an anisotropic g tensor, anisotropic linewidths along the principal directions and Lorentzian lineshape using the program MONOQF (Fig. 7). The results of the simulation together with the integral intensity $I(T)$ are presented in Fig. 8. The g tensor exhibited rhombic symmetry with principal g_i values ($i=x, y, z$) only slightly temperature dependent. Namely, the obtained g_i values are found to be in the range $g_x=2.040-2.043$, $g_y=2.115-2.1145$, $g_z=2.230-2.228$, where the first value corresponds to the lowest temperature (3.8 K) and the second to the highest studied temperature (49 K) [Fig. 8(a)]. The relation $g_z>g_y>g_x$ among the principal g values indicates that the underlying Cu^{2+} centers have a dominant $d_{x^2-y^2}$ and to a lesser extent a d_z^2 contribution in their ground state, corresponding to a rhombic distortion of the local symmetry. The linewidths turned out to be anisotropic, following relation $\Delta H_z\sim\Delta H_y>\Delta H_x$ which is consistent with the dipolar contribution to ΔH_i ($i=x, y, z$) predicted by the principal g_i values. As the temperature decreased, especially below 10 K, an increase of ΔH_i of the order of 25 MHz$\sim$10 G is observed [Fig. 8(b)]. Analysis of the integral intensity as a function of temperature reveals that $I(T)$ does not increase as T^{-1} upon lowering the temperature, but rather with an $T^{-0.82}$ law for most of the investigated temperature range or alternatively with a Curie-Weiss law $C/(T-\Theta)$ with negative Θ values [Fig. 8(c)]. This antiferromagnetic behavior can be more readily traced in the plot $I\times T$ vs T [Fig. 8(c)], where $I\times T$ decreases continuously below $T=30$ K though below 5 K an increase of $I\times T$ is detected. In this case, both the EPR intensity and the linewidth temperature variation strongly suggest that the underlying copper centers are not ''isolated'' but rather exhibit substantial magnetic interactions of antiferromagnetic character.

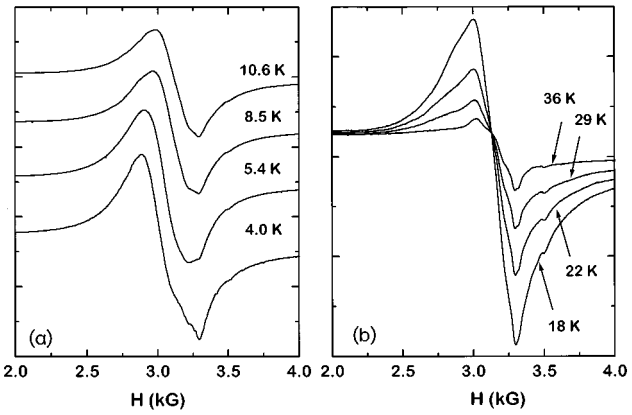

FIG. 9. Temperature dependence of the EPR spectra for the (Nd,Y)123 sample (B) recorded immediately after preparation at (a) $T<10$ K and (b) $T>10$ K.

Impurity copper oxides such as $BaCuO_{2+x}$ and the ''green'' R_2BaCuO_5 phase have been found to exhibit anisotropic Cu^{2+} EPR spectra with principal g values, though not identical, in the same g range as in the present case.[1,39,40] However, these Cu^{2+} EPR spectra are usually much broader than the present ones, while they have not been reported to exhibit similar temperature as that reported in Fig. 8. Moreover, the present EPR spectra bear close resemblance to those recently reported for oxygen deficient $YBa_2Cu_3O_{7-\delta}$ samples, especially that reported for $\delta=0.3$, which were directly related to the appearance of the anomalous microwave absorption (MWA).[41] In that case, the EPR spectra were attributed to Cu^{2+} impurity ions in the Cu(1) chains providing the π junctions implicated in the anomalous MWA.[41] In this respect, we consider that the rhombic Cu^{2+} EPR spectra detected in the Sm123 sample B have an intrinsic character. Based on the observed reduction of the EPR intensity compared to that of the isotropic EPR line (sample A), we suggest that the increase of oxygen deficiency or oxygen ordering might cause a ''dilution'' of the ferromagnetic phase evidenced in samples A and give rise to more ''isolated'' Cu^{2+} centers which, however, exhibit antiferromagnetic interactions.

Subsequently, we present the results of the EPR study of a mixed $Nd_{0.5}Y_{0.5}Ba_2Cu_3O_{6+x}$ (Nd,Y)123 oxygen deficient sample B, which was chosen for two purposes: (a) to reduce the Nd concentration which might enable the detection of the Nd^{3+} EPR resonance that was not detected in the single Nd123 sample, and (b) to verify that heat treatment of samples B results in the radical changes of the copper EPR spectra as observed in the Sm123 samples. The EPR spectra of the (Nd,Y)123 sample recordered immediately after preparation, as for all samples presented so far, is shown as a function of temperature in Fig. 9. At temperatures below 10 K [Fig. 9(a)], the EPR spectrum has an unusual shape, especially in the high-field side where some structure appears, while a small shift of the resonance line can be traced, similar to the $g_{\rm eff}(T)$ of the isotropic EPR line in sample Sm123 (A) (Fig. 5). However, as temperature increases some characteristic features of the type expected for anisotropic powder EPR spectra of Cu^{2+} ions, similar to the Cu^{2+} EPR spectra of Sm123 (B), gradually become resolved [Fig. 9(b)]. In this case, it seems that the detected EPR spectrum is the

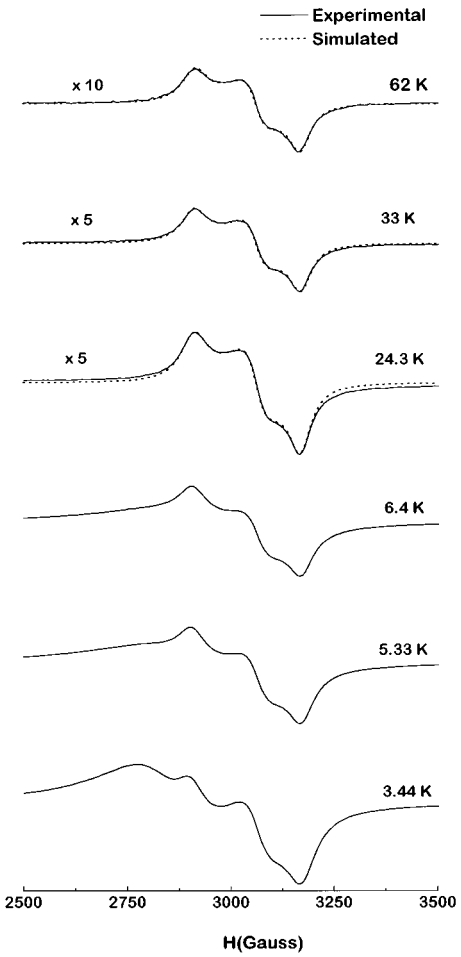

FIG. 10. Temperature dependence of the EPR spectra (solid lines) for the ''aged'' (Nd,Y)123 sample (B) after a time period of 5 months. The dotted lines represent the simulated EPR spectra at relatively high temperatures.

result of the superposition of two different EPR signals, most probably of the form detected in the Sm123 samples (A) and (B).

EPR measurements were repeated for the same (Nd,Y)123 sample after five months. During this time period the sample was kept sealed in the same quartz tube as measured for the first time. The motivation for such a measurement were previous observations of substantial time evolution of the copper EPR spectra in $Pr_{0.5}R_{0.5}Ba_2Cu_3O_{6+x}$ ceramics.[42,43] The EPR spectra of the ''aged'' (Nd,Y)123 sample (B) at some temperatures are shown in Fig. 10. At higher temperatures the EPR spectrum is dominated by an anisotropic powder EPR pattern of Cu^{2+} ions with rhombic g tensor similar to that observed in Sm123 (B), while at lower temperatures it results from the superposition of the Cu^{2+} EPR spectrum with a more isotropic EPR signal which rapidly intensifies upon lowering the temperature. Deconvolution of the EPR spectrum was performed by simulating the rhombic Cu^{2+} EPR.

The Cu^{2+} EPR spectrum can be accurately simulated down to ~20 K with a rhombic g tensor with constant principal values $g_x=2.070(1)$, $g_y=2.143(1)$, $g_z=2.253(1)$ and anisotropic linewidths, $\Delta H_x=85$ MHz, $\Delta H_y=107$ MHz, $\Delta H_z=118$ MHz at $T=62$ K slightly increasing (by ~3–5 MHz) with decreasing temperature down to 20 K (Fig. 10).

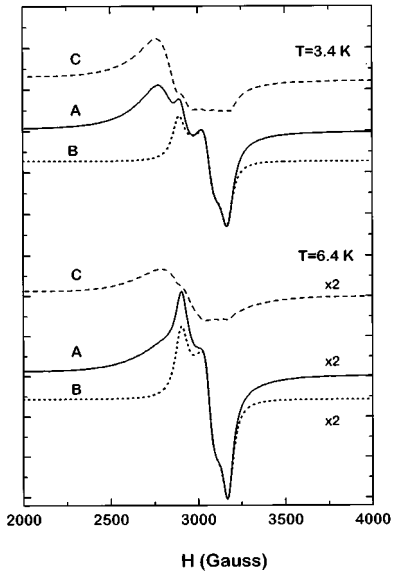

FIG. 11. Deconvolution of the EPR spectrum of the ''aged'' (Nd,Y)123 sample (B) at low temperatures of 3.4 and 6.4 K. A designates the initial spectrum, B the simulated Cu^{2+} EPR spectrum, and C the more isotropic EPR spectrum obtained from the subtraction of A-B.

In the temperature range $T=3.44-20$ K the g_y, g_z values exhibit a gradual change reaching the values of 2.140 and 2.268 at $T=3.44$, while the linewidth continues to increase similarly to the Sm123 sample (B) [Fig. 8(b)] reaching the largest values $\Delta H_x=103$ MHz, $\Delta H_y=119$ MHz, $\Delta H_z=130$ MHz at $T=3.44$ K. Additionally, the integral intensity $I(T)$ increases slower than T^{-1} with decreasing temperature, similar to the temperature variation of the Cu^{2+} EPR spectrum of sample Sm123 (B) [Fig. 8(c)].

The more isotropic EPR component was obtained after subtraction of the Cu^{2+} EPR spectrum from the total EPR spectrum at low temperatures ($T<7$ K), as can be seen in Fig. 11. Although, the high-field part of this EPR spectrum can not be accurately retrieved, its shape resembles closely the isotropic EPR line detected in samples (A). This also supported by the temperature variation of the derived spectrum, namely the faster than T^{-1} increase of its intensity $I(T)$ as well as the increase of the $g_{\rm eff}$ value as the temperature decreases, which are both characteristics of the isotropic EPR line detected in samples (A) [Figs. 6(a) and 6(c)].

These results suggest that during the time period of 5 months, a substantial increase of the intensity of the rhombic Cu^{2+} EPR spectrum occurred relatively to the isotropic EPR line. This effect along with the different $I(T)$ variation of the two EPR spectra allowed their decomposition for the aged (Nd,Y)123 sample (B). Additionally, the EPR results for the (Nd,Y) sample support our observation that increase of the high-temperature He-annealing time reduces the concentration of the ferromagnetic copper clusters responsible for the isotropic EPR line and favors the formation of more ''isolated'' Cu^{2+} centers giving rise to the rhombic EPR spectrum.

C. Electron paramagnetic resonance of Nd^{3+} and Sm^{3+} ions

In all of the studied samples, we did not observe any appreciable indication of the EPR signals resulting from the

TABLE III. The principal EPR g_i values and the corresponding secular second moment $M_{20}^{(i)}$ $(i=x, y, z)$ due to the magnetic dipolar interactions of Nd^{3+} and Sm^{3+} ions in $RBa_2Cu_3O_{6+x}$ (R=Nd, Sm) compounds.

	g_x	g_y	g_z	$M_{20}^{(x)}$ (kG)^2	$M_{20}^{(y)}$ (kG)	$M_{20}^{(z)}$ (kG)^2
$NdBa_2Cu_3O_7$	2.83	2.20	2.49	3.71	3.04	1.56
$NdBa_2Cu_3O_{6.1}$	2.46	2.46	2.18	2.92	2.92	1.12
$SmBa_2Cu_3O_{6+x}$	0.63	0.63	0.53	0.056	0.056	0.024

paramagnetic rare-earth Nd^{3+} and Sm^{3+} *Kramers* ions, though their paramagnetic contribution determines largely the bulk magnetic properties of the respective $R123$ compounds. On the other hand, all the other R^{3+} Kramers ions (R=Gd, Dy, Er, Yb) forming the $R123$ compounds have been found to produce detectable EPR signals, though considerably broadened in the case of Er^{3+} and Dy^{3+}, in the X band.[44] Moreover, analysis of these R^{3+} EPR spectra showed that they occur at g values close to that predicted by the CF ground doublets and most importantly that the linewidth in the single $R123$ matrix is mainly determined by the magnetic interactions (dipolar and exchange) of the R^{3+} ions.[44] In this respect, we give below a brief account of the Nd^{3+} and Sm^{3+} EPR resonance based on the previous CF analysis hoping to stimulate future EPR studies on these R^{3+} ions.

As is well known, for Nd^{3+} and Sm^{3+} ions in D_{2h} and D_{4h} CF symmetry occurring in the $R123$ crystal structure, the EPR spectrum of the R^{3+} ground doublet is described by an anisotropic g tensor whose principal components can be straightforwardly calculated.[45] The principal g_i values $(i=x, y, z)$ where the x, y, z principal axes can be identified with the a, b, c crystallographic axes, are presented in Table III. In the case of the orthorhombic $NdBa_2Cu_3O_7$ compound the ground doublet has been derived by CF calculation in the D_{2h} symmetry and using the CF parameters reported by Goodman, Loong, and Soderholm,[46] while in the tetragonal symmetry of Nd123 and Sm123 the CF states derived by H_{CF} (1) were used.

Furthermore, for the undiluted $R123$ compounds we have numerically calculated the contribution of the dipolar interaction in the second moment M_2 of the Nd^{3+} EPR resonance in the high-temperature approximation taking into account the anisotropy of the g_i values explicitly.[44] Due to the relatively large distance of the rare-earth layers along the c axis, we have considered only the R^{3+} ions lying in the same ab plane. The results are included in Table III, where $M_{20}^{(i)}$ are the values of the secular second moment arising from the truncated dipolar Hamiltonian with the magnetic field along the x, y, z axes. If the linewidth was determined solely by the dipolar interaction, the resonance would have Gaussian line shape with peak-to-peak linewidth $\Delta H_{pp}^{(i)}=2\sqrt{M_{20}^{(i)}}$.[47]

In the case of Nd^{3+} ions it is seen that the g_i values are not very anisotropic and are well within the X-band range, while the dipolar linewidths are approximately 3.4 and 2.1 kG along the x, z axes in the tetragonal symmetry. The resulting powder Nd^{3+} EPR spectrum, though broad can be easily detected in the X band. If we assume isotropic exchange interaction J among the real Nd^{3+} spins and project on the ground doublet, we derive an isotropic interaction of magnitude $J_{iso}\approx 0.75J-0.02$ cm^{-1}. The latter contributes in the fourth moment M_4 causing narrowing of the resonance line whose width is then given by $\Delta H_{(i)}=M_{20}^{(i)}/\nu_{ex}$, where ν_{ex} is the exchange frequency. Assuming a small value of $J=0.01$ cm^{-1} and using the expression for the fourth moment recently reported by Deville *et al.*,[48] we derive the ν_{ex} values of 3135 and 2050 MHz along the x and z axes. These ν_{ex} values, which are smaller than the resonance frequencies (adiabatic approximation), along with the $M_{20}^{(i)}$ values in the tetragonal Nd123 (Table III), finally give linewidths $\Delta H_x=0.93$ kG and $\Delta H_z=0.55$ kG. The latter values are smaller than the initial dipolar linewidths, while they can be even smaller when larger exchange values J are used. At this point it should be noted that the contribution in the second moment of the isotropic exchange interaction J is not zero but very small due to the small anisotropy of the g_i values. Moreover, contribution of the hyperfine structure of the natural Nd isotopes in the second moment is about an order of magnitude smaller than the dipolar one,[44] while a significant broadening contribution may arise through the anisotropic exchange interaction of Nd^{3+} ions. However, in all cases it seems unlikely that the magnetic interactions excessively broaden the Nd^{3+} EPR spectrum beyond the X-band range. This is also supported by the absence of a definite Nd^{3+} EPR signal in the (Nd,Y)123 sample where the dilution of Nd^{3+} should considerably reduce the magnetic interactions and thus EPR broadening.

In the case of the Sm^{3+} ions, the predicted g_i values (Table III) are as usual rather small and correspond to resonance fields of $H_x=10.7$ kG and $H_z=12.7$ kG assuming $\nu_0=9.43$ GHz. Although the latter values approach the limit of our magnetic-field range (0–11 kG), EPR measurements in magnetic field up to 11 kG in the Sm123 samples did not gave any sign of resonance signal. The predicted dipolar linewidths are quite small $\Delta H_{pp}^{(x)}=0.47$ kG, $\Delta H_{pp}^{(z)}=0.31$ kG and become even smaller in the presence of exchange interactions. Based on this analysis, we conclude that the EPR resonance of Sm^{3+} and Nd^{3+} in contrast with the heavier Kramers R^{3+} ions is significantly broadened by spin-lattice-relaxation processes. This behavior may be considered to some extend plausible, if we take into account the larger ion radius of Nd^{3+} and Sm^{3+} which allows for larger coupling with the crystal lattice. However, it is worth investigating the dynamic behavior of these R^{3+} ions which are very close to Pr^{3+} which as is well known cause the disappearance of superconductivity in the $PrBa_2Cu_3O_7$ compound. In this respect, high-frequency EPR measurements would probably enable the detection and study of the Nd^{3+} and Sm^{3+} EPR spectra.

IV. DISCUSSION

Both the magnetization and the EPR results strongly suggest the presence of a small but substantial ferromagnetic (FM) contribution most probably related with local FM clusters in the nonsuperconducting oxygen deficient $RBa_2Cu_3O_{6+x}$ (R=Nd, Sm) compounds. Furthermore, it is very interesting to examine the origin of this behavior in relation to the magnetic behavior of the $R123$ systems as a function of the oxygen concentration.

Introduction of oxygen in the antiferromagnetic $YBa_2Cu_3O_6$ compound is initially ($0<x<0.2$) expected to result in random filling of isolated vacancies in the basal Cu(1) layer giving rise to Cu^{2+}-O^{2-}-Cu^{2+} dimers.[11] However, AFM exchange coupling of the two Cu^{2+} ions of similar magnitude ($J\sim10^3$ K) as in the Cu(2) planes, would leave the singlet ($S=0$) as a ground state and thus turn these dimers to nonmagnetic up to high temperatures. Further introduction of oxygen induces holes O^- with spin 1/2, which are predicted to remain incorporated in short chain fragments in the Cu(1) layer, before any charge transfer to the Cu(2) takes place.[11] In these neutral Cu(1) chain fragments there is an even number of spins (for N oxygen sites, there are $N-1$ oxygen holes and $N+1$ copper holes, thus $2N$ spins) which assuming AFM exchange coupling among all spins leads to a singlet ground state.[12] However, if the oxygen hole occupies the $p\pi$ orbital, then strong ferromagnetic coupling ($J\sim+400$ K) between the oxygen $p\pi$ and adjacent copper d orbitals prevails.[49] In this case, ground state of the short Cu(1) fragments with total spin $S>1/2$ may arise. These Cu(1) chain fragments are predicted to have a critical length (~3 oxygens per fragment) before holes are induced in the Cu(2) planes. Such FM clusters appearing in the Cu(1) layer most favorably at oxygen concentration slightly lower than that corresponding to the superconducting phase transition, could probably explain the observed isotropic EPR spectra. Morever, due to the orthogonality of the $d_{y^2-z^2}$ orbital of $Cu^{2+}(1)$ ions with the $d_{x^2-y^2}$ orbitals of $Cu^{2+}(2)$ ions, ferromagnetic exchange interaction between $Cu^{2+}(1)$ and $Cu^{2+}(2)$ along the c axis may also occur. A theoretical estimate of the latter interaction yields $J_{\mathrm{Cu(1)\text{-}Cu(2)}}\sim+10$ K,[49] which is very close to the temperature where the resonance frequency and the EPR linewidth start to diverge [Figs. 6(b) and 6(c)]. Another possibility for the detection of EPR signals from Cu(1) chain fragments even in the presence of overall AFM coupling, is the presence of the loosely coupled $Cu^{2+}(1)$ magnetic moments at the end of such chain fragments as previously suggested in Ref. 20, in order to explain the oxygen dependence of the ^{169}Tm nuclear spin-lattice-relaxation time. In this case, $Cu^{2+}(1)$ copper centers coupled ferromagnetically with $Cu^{2+}(2)$ may be responsible for the isotropic EPR spectra.

However, ferromagnetic copper clusters may also arise in the AFM Cu(2) planes when lightly doped with oxygen holes. Recently, the low-energy spectrum of two different spin-polarized clusters where the oxygen hole is allowed to move freely, was examined.[17] The first was a pentanuclear copper cluster which was found to have a ground state with total spin $S=2$.[17] The latter state was estimated to be split by the anisotropic exchange interaction of the oxygen hole with the copper spins, in one singlet $M_s=0$ as the ground state and two *non-Kramers* doublets with quantum numbers M_s equal to ±1 and ±2 at energies 0.6–2.3 K and 2.3–9.3 K, respectively. EPR signal from the non-Kramers doublets is not easily detectable, while EPR transitions among the $M_s=0$ and the $M_s=\pm1$ energy states which may be quite close in energy (0.4–1.6 cm^{-1}), are not very likely to occur at the X band, though, in principle, it may be possible at higher frequencies. The second cluster was a tetranuclear copper cluster where the oxygen hole was confined in the b_{2g} orbital.[17] In this case, the cluster ground state has total spin $S=3/2$ which is further split by anisotropic exchange into two Kramers doublets with energy separation of 60–230 K.[17] This kind of spin-polarized cluster has been considered to be responsible for the EPR signal detected in $La_2CuO_{4+\delta}$ and is also a possible candidate for the present EPR signals. However, the EPR signal detected in $La_2CuO_{4+\delta}$ showed a marked increase of $I\times T$ with decreasing temperature below 25 K but no g-shift or linewidth increase as in the $R123$ oxygen deficient samples which exhibited a more complicated behavior. If this kind of spin-polarized cluster is responsible for the isotropic EPR line in the $R123$ systems, it may be possible that the low-temperature EPR behavior involves interaction of these clusters with the $Cu^{+2}(1)$ moments, rather than intercluster interactions which should be rather weak due to their small concentration. Is also very interesting to note that any cluster formation either in the Cu(1) or Cu(2) layers may occur in a wider oxygen concentration range in $RBa_2Cu_3O_{6+x}$ (R=Nd, Sm) where the large rare-earth ion radius was found to shift the orthorhombic-to-tetragonal phase transition at $x=0.55$ which is considerably higher than in the $YBa_2Cu_3O_{6+x}$ system.[50]

On the other hand, the remarkable disappearance of the intense, isotropic EPR line and the substantial magnetization reduction after increasing the high-temperature annealing time, are indicative of a ''dilution'' effect of the FM phase which normally is expected to occur for further increase of the oxygen deficiency. The latter inhibits the formation of Cu(1) and mostly Cu(2) clusters by decreasing sufficiently the number of available oxygen holes. The appearance of the rhombic Cu^{2+} EPR spectra and their temperature dependence indicate the presence of more ''isolated'' Cu^{2+} centers with relatively weak antiferromagnetic interactions. The time-induced growth of the intensity of this EPR spectrum, as evidenced in the (Nd,Y)123 sample, may be related to slow oxygen ordering processes occurring in the 123 crystal structure as has been suggested in Ref. 51. However, it may also be related with surface states, since the surface of the 123 ceramics has been found to be most susceptible to environmental degradation.[52]

In summary, our magnetic and EPR data suggest the formation of ferromagnetic copper clusters in oxygen deficient, nonsuperconducting $RBa_2Cu_3O_{6+x}$ ceramics containing the relatively large rare-earth ions Nd^{3+} and Sm^{3+}. Their origin can be traced in the spin polarization of divalent copper ions through oxygen holes either in the Cu(1) or in the Cu(2) layers, while the ferromagnetic interaction of the Cu(1) with the Cu(2) moments may play an important role in the divergent behavior of the EPR parameters at low temperatures ($T<10$ K). On increasing the oxygen deficiency of the samples, the ferromagnetic contribution is drastically reduced and more isolated Cu^{2+} centers with relatively weak antiferromagnetic interactions appear. Additionally, linewidth analysis of the EPR spectra of Nd^{3+} and Sm^{3+} ions based on the CF energy states, indicate that the absence of the Nd^{3+} and Sm^{3+} EPR resonance is most likely due to very fast spin lattice in contrast with the other R^{3+} Kramers ions whose EPR linewidth is mainly determined by their magnetic interactions.

ACKNOWLEDGMENTS

We would like to thank Professor J. R. Pilbrow for providing us with the MONOQF simulation program and Dr. V. Petrouleas for arranging the EPR measurements.

*Corresponding author.
[1] A. Punnoose and R. J. Singh, J. Math. Phys. **35**, 1123 (1994).
[2] W. E. Farneth, R. S. McLean, E. M. McCarron III, F. Zuo, Y. Lu, B. R. Patton, and A. J. Epstein, Phys. Rev. B **39**, 6594 (1989).
[3] Y. Yamaguchi, S. Waki, and M. Tokumoto, Solid State Commun. **69**, 1153 (1989).
[4] X. Obradors, J. Tejada, J. Rodriguez, F. Perez, M. Vallet, J. Gonzales-Calbet, and M. Medarde, J. Magn. Magn. Mater. **83**, 517 (1990).
[5] F. Zuo, A. J. Epstein, E. M. McCarron III, and W. E. Farneth, Physica C **167**, 567 (1990).
[6] I. M. Fita, N. A. Doroshenko, V. P. D'yakonov, E. E. Zubov, G. G. Levchenko, and V. I. Markovich, Sov. Phys. Solid State **34**, 1371 (1992).
[7] V. P. D'yakonov, E. E. Zubov, G. G. Levchenko, V. I. Markovich, I. M. Fita, and N. A. Doroshenko, Sov. Phys. Solid State **33**, 1848 (1992).
[8] H. Gamari-Seale, N. Guskos, A. Koufoudakis, I. Kruk, C. Mitros, V. Likodimos, N. Niarchos, and V. Psyharis, Philos. Mag. B **65**, 1381 (1992).
[9] N. Guskos, G. P. Triberis, V. Likodimos, A. Kondos, A. Koufoudakis, C. Mitros, H. Gamari-Seale, and D. Niarchos, Phys. Status Solidi B 164, K105 (1991).
[10] N. Guskos, V. Likodimos, C. A. Londos, W. Windsch, H. Metz, A. Koufoudakis, C. Mitros, H. Gamari-Seale, and D. Niarchos, Phys. Status Solidi B **170**, 597 (1992).
[11] G. Uimin and J. Rossat-Mignod, Physica C **199**, 251 (1992).
[12] A. O. Gogolin and A. S. Ioselevich, JETP Lett. **53**, 375 (1991).
[13] A. Aharony, R. J. Birgeneau, A. Coniglio, M. A. Kastner, and H. E. Stanley, Phys. Rev. Lett. **60**, 1330 (1988).
[14] V. Hizhnyakov and E. Sigmund, Physica C **156**, 655 (1988).
[15] G. Seibold, E. Sigmund, and V. Hizhnyakov, Phys. Rev. B **48**, 7537 (1993).
[16] D. N. Aristov and S. V. Maleyev, Z. Phys. B **93**, 181 (1994).
[17] M. V. Eremin and E. Sigmund, Solid State Commun. **90**, 795 (1994).
[18] G. Wubbeller and O. F. Shirmer, Phys. Status Solidi B **174**, K21 (1992).
[19] P. G. Baranov and A. G. Badalyan, Solid State Commun. **85**, 987 (1993); Physica C **235–240**, 267 (1994).
[20] O. N. Bakharev, A. G. Volodin, A. V. Duglav, A. V. Egorov, O. B. Marvin, V. V. Naletov, M. A. Teplov, and D. Wagner, JETP Lett. **58**, 630 (1993).
[21] O. N. Bakharev, J. Witteveen, H. B. Brom, E. V. Krjukov, O. B. Marvin, and M. A. Teplov, Phys. Rev. B **51**, 693 (1995).
[22] K. N. Yang, J. M. Ferreira, B. W. Lee, M. B. Maple, W.-H. Li, J. W. Lynn, and R. W. Erwin, Phys. Rev. B **40**, 10 963 (1989); T. W. Clinton, J. W. Lynn, B. W. Lee, M. Buchgeister, and M. B. Maple, J. Appl. Phys. **73**, 6320 (1993).
[23] P. Allenspach, M. B. Maple, and A. Furrer, J. Alloys Compounds **207/207**, 213 (1994).
[24] B. G. Wybourne, *Spectroscopic Properties of Rare Earths* (Wiley, New York, 1965).
[25] P. Allenspach, J. Mesot, U. Staub, A. Furrer, H. Blank, H. Mutka, R. Osborn, A. Taylor, H. Maletta, M. J. Kramer, S. I. Yoo, E. Kaldis, J. Karpinski, and S. Rusiecki, Physica B **180&181**, 389 (1992).
[26] B. G. Wybourne, J. Chem. Phys. **34**, 279 (1961); H. M. Crosswhite, H. Crosswhite, F. W. Kaseta, and R. Sarup, *ibid.* **63**, 1981 (1976).
[27] J. H. Van Vleck, *The Theory of Electric and Magnetic Susceptibilities* (Oxford University Press, Oxford, 1932).
[28] D. C. Johnston, J. Magn. Magn. Mater. **100**, 218 (1991).
[29] L. Soderholm, W.-K. Kwok, G. L. Goodman, and C.-K. Loong, Eur. J. Solid State Inorg. Chem. **28**, 615 (1991).
[30] C. A. Morrison and R. P. Leavitt, J. Chem. Phys. **71**, 2366 (1979).
[31] V. Nekvasil, Solid State Commun. **65**, 1103 (1988).
[32] B. G. Wybourne, J. Chem. Phys. **36**, 2301 (1962).
[33] N. Guskos, V. Likodimos, C. A. Londos, V. Psycharis, C. Mitros, A. Koufoudakis, H. Gamari-Seale, W. Windsch, and H. Metz, J. Solid State Chem. **119**, 50 (1995).
[34] Z.-R. Wang, X.-L. Wang, J. A. Fernandez-Baca, D. C. Johnston, and D. Vaknin, Science **264**, 402 (1994).
[35] A. Bencini and D. Gatteschi, *Electron Paramagnetic Resonance of Exchange Coupled Systems* (Springer-Verlag, Berlin, 1990).
[36] R. D. Willett and F. Waldner, J. Appl. Phys. **53**, 2680 (1982).
[37] T. Karasudani and H. Okamoto, J. Phys. Soc. Jpn. **43**, 1131 (1977).
[38] R. Troc, J. Janicki, A. Zygmunt, H. Drulis, and A. Niedzwiedz, Physica B **193**, 1 (1994).
[39] R. N. de Mesquita, J. H. Castilho, G. E. Barberis, C. Rettori, I. Torriani, O. F. de Lima, S. Gamma, R. F. Jardim, M. C. Terrile, H. Basso, and O. R. Nacsimento, Phys. Rev. B **39**, 6694 (1989).
[40] R. Jones, R. Janes, R. Armstrong, N. C. Pyper, P. P. Edwards, D. J. Keeble, and M. R. Harrison, J. Chem. Soc. Faraday Trans. **86**(4), 675 (1990). .
[41] S. V. Bhat, A. Rastogi, N. Kumar, R. Nagarajan, and C. N. Rao, Physica C **219**, 87 (1994).
[42] N. Guskos, V. Likodimos, S. K. Patapis, J. Kuriata, M. Wabia, L. Sadlowski, A. Koufoudakis, C. Mitros, H. Gamari-Seale, and V. Psyharis, Phys. Status Solidi B **184**, 445 (1994).
[43] V. Likodimos, N. Guskos, G. Palios, A. Koufoudakis, J. Typek, B. Bojanowski, and M. Wabia, , Phys. Rev. B **52**, 7682 (1995).
[44] V. Likodimos, Ph.D. thesis, University of Athens, Athens, 1996.
[45] J. M. Baker, Electron Spin Reson. **138**, XX (1993).
[46] G. L. Goodman, C.-K. Loong, and L. Soderholm, J. Phys. Condens. Matter **3**, 49 (1991); L. Soderholm, C.-K. Loong, G. L. Goodman, and B. D. Dabrowski, Phys. Rev. B **43**, 7923 (1991).
[47] J. H. Van Vleck, Phys. Rev. **74**, 1168 (1948); P. W. Anderson and P. R. Weiss, Rev. Mod. Phys. **25**, 269 (1953).
[48] A. Deville, L. Bejjit, B. Gaillard, J. P. Sorbier, O. Monnereau, H. Noel, and M. Potel, Phys. Rev. B **47**, 2840 (1993).
[49] Y. Guo, J. M. Langlois, and W. A. Goddard III, Science **239**, 897 (1988).
[50] H. Shaked, B. W. Veal, J. Faber, Jr, R. L. Hitterman, U. Balachandran, G. Tomlins, H. Shi, L. Morss, and A. P. Paulikas, Phys. Rev. B **41**, 4173 (1990).
[51] S. Semenovskaya and A. G. Khachaturyan, Phys. Rev. B **46**, 6511 (1992).
[52] R. Zhao and S. Myhra, Physica C **230**, 75 (1994).